PLOS ONE

RESEARCH ARTICLE

Quantitative systems pharmacology of interferon alpha administration: A multi-scale approach

Priyata Kalra[1], Julian Brandl[1,2], Thomas Gaub[3], Christoph Niederalt[3], Jörg Lippert[3], Sven Sahle[1], Lars Küpfer[3], Ursula Kummer[1]*

1 Department of Modelling of Biological Processes, COS/BioQuant, Heidelberg University, Im Neuenheimer Feld 267, Heidelberg, Germany, **2** Now at Department of Systems Biology, Technical University of Denmark, Kgs. Lyngby, Denmark, **3** Clinical Sciences, Bayer Pharma, Kaiser-Wilhelm-Allee 1, Leverkusen, Germany

* ursula.kummer@bioquant.uni-heidelberg.de

OPEN ACCESS

Citation: Kalra P, Brandl J, Gaub T, Niederalt C, Lippert J, Sahle S, et al. (2019) Quantitative systems pharmacology of interferon alpha administration: A multi-scale approach. PLoS ONE 14(2): e0209587. https://doi.org/10.1371/journal.pone.0209587

Editor: Wenyu Lin, Harvard Medical School, UNITED STATES

Received: July 2, 2018

Accepted: December 8, 2018

Published: February 13, 2019

Data Availability Statement: All relevant data are within the paper and its Supporting Information files and in referenced literature.

Funding: This research was supported by Bundesministerium für Bildung und Forschung (ImmunoQuant to UK) and (LiSym 031L0039 to LK). Four of the authors (LK, TG, CN, JL) are employees of Bayer Pharma. However, the funder/company did not have any additional role in the study design, data collection and analysis, decision to publish, or preparation of the manuscript.

Abstract

The therapeutic effect of a drug is governed by its pharmacokinetics which determine the downstream pharmacodynamic response within the cellular network. A complete understanding of the drug-effect relationship therefore requires multi-scale models which integrate the properties of the different physiological scales. Computational modelling of these individual scales has been successfully established in the past. However, coupling of the scales remains challenging, although it will provide a unique possibility of mechanistic and holistic analyses of therapeutic outcomes for varied treatment scenarios. We present a methodology to combine whole-body physiologically-based pharmacokinetic (PBPK) models with mechanistic intracellular models of signal transduction in the liver for therapeutic proteins. To this end, we developed a whole-body distribution model of IFN-*α* in human and a detailed intracellular model of the JAK/STAT signalling cascade in hepatocytes and coupled them at the liver of the whole-body human model. This integrated model infers the time-resolved concentration of IFN-*α* arriving at the liver after intravenous injection while simultaneously estimates the effect of this dose on the intracellular signalling behaviour in the liver. In our multi-scale physiologically-based pharmacokinetic/pharmacodynamic (PBPK/PD) model, receptor saturation is seen at low doses, thus giving mechanistic insights into the pharmacodynamic (PD) response. This model suggests a fourfold lower intracellular response after administration of a typical IFN-*α* dose to an individual as compared to the experimentally observed responses in *in vitro* setups. In conclusion, this work highlights clear differences between the observed *in vitro* and *in vivo* drug effects and provides important suggestions for future model-based study design.

Competing interests: LK, TG, CN, JL are employees of Bayer Pharma, Germany. This does not alter our adherence to PLOS ONE policies on sharing data and materials.

Introduction

Pleiotropic interferon alpha (IFN-α) belongs to the type I IFNs family. IFN-α is an extensively used cytokine in clinical medicine, effective in hepatitis C (HCV) and hepatitis B (HBV) treatment over the past 20 years [1–9]. Despite its routine application in clinical practice [10], there is incomplete understanding regarding its modes of action and the causality of induced pharmacodynamic effects. Therefore, hepatocytes have become important *in vitro* study models for IFN-α action [11]. One hindrance to discern the molecular response in hepatocytes to IFN-α treatment is that the experimental investigation requires liver biopsies of patients undergoing IFN-α therapy. This is ethically difficult, if not infeasible and would impose a significant burden for the patient [12].

IFN-α canonically acts via the JAK/STAT pathway (Fig 1). IFN binds to the interferon receptor subunits IFNAR1 and IFNAR2 to form a heterodimeric ligand receptor complex. This heterodimeric ligand receptor complex activates intracellular signalling via the receptor associated kinases Tyk2 and JAK1, which mutually phosphorylate each other. STAT1 and STAT2 molecules associate with the receptor complex and form a phosphorylated heterodimer. The phosphorylated heterodimer of pSTAT1/2 is released from the receptors to form the hetero-trimeric ISGF3 transcription factor by binding IRF-family member IRF9 (p48/ISGF3). ISGF3 translocates into the nucleus and activates the interferon-stimulated response elements (ISRE). The activated ISREs lead to the expression of various antiviral proteins like Mx1, Mx2 and RNA-dependent protein kinase (PKR) [13]. The pathway exerts several negative feedbacks that result in a strong regulation of the interferon-stimulated genes (ISGs). SOCS (suppressors of cytokine signalling), PIAS (protein inhibitors of activated stats) and PTPs (protein tyrosine phosphatases) are among the most important negative regulators of the pathway. Genes for SOCS and IRF9 can contain both GAS and ISRE as transcription factor binding sites and are therefore activated by IFN dependent signalling.

On the pharmaceutical side, IFN-α pharmacokinetics are fairly well described. A significant inter-individual variability is well known from clinical practice [14, 15]. In the future, personalised treatment scenarios might arise from the deeper understanding of the detailed mechanisms of IFN-α action and inter-individual patient variability, improving success rates of IFN-based therapies [16–18]. In order to gain an integrative and profound understanding of IFN-α drug action, we use a quantitative systems pharmacology (QSP) approach which simultaneously considers multiple levels of biological organisation [19]. For this purpose, we integrated a detailed cellular model of IFN-α signalling through the JAK/STAT pathway [20] into a physiologically-based pharmacokinetic (PBPK) model at the whole-body scale [21, 22] for healthy humans. Thus, it was possible to simultaneously describe IFN-α pharmacokinetics as well as the resulting drug-induced response, i.e. the pharmacodynamics (PD), within one integrated multi-scale model representation.

Computational models of intracellular signalling pathways have been previously developed to describe IFN-α induced responses in the cellular signalling network [20, 23–28]. To calibrate these non-linear ODE-models, quantitative data which are primarily generated under controlled *in vitro* conditions such as cell cultures (reviewed in [29]) or tissue cultures [30], are needed. However, many *in vitro* assays only allow stationary concentration profiles in contrast to the highly dynamic PK concentration profiles occurring *in vivo*. On the contrary, the integration of cellular models within whole-body PBPK models provides the unique opportunity to simulate cellular responses to IFN-α stimuli within an *in vivo* context. We present a multi-scale PBPK/PD model that simultaneously quantifies the amount of IFN-α reaching the liver in a time-resolved manner, as well as the induced response in the intracellular signalling network. Ultimately, administration of IFN-α leads to the expression of IRF9 mRNAc (Fig 2). To

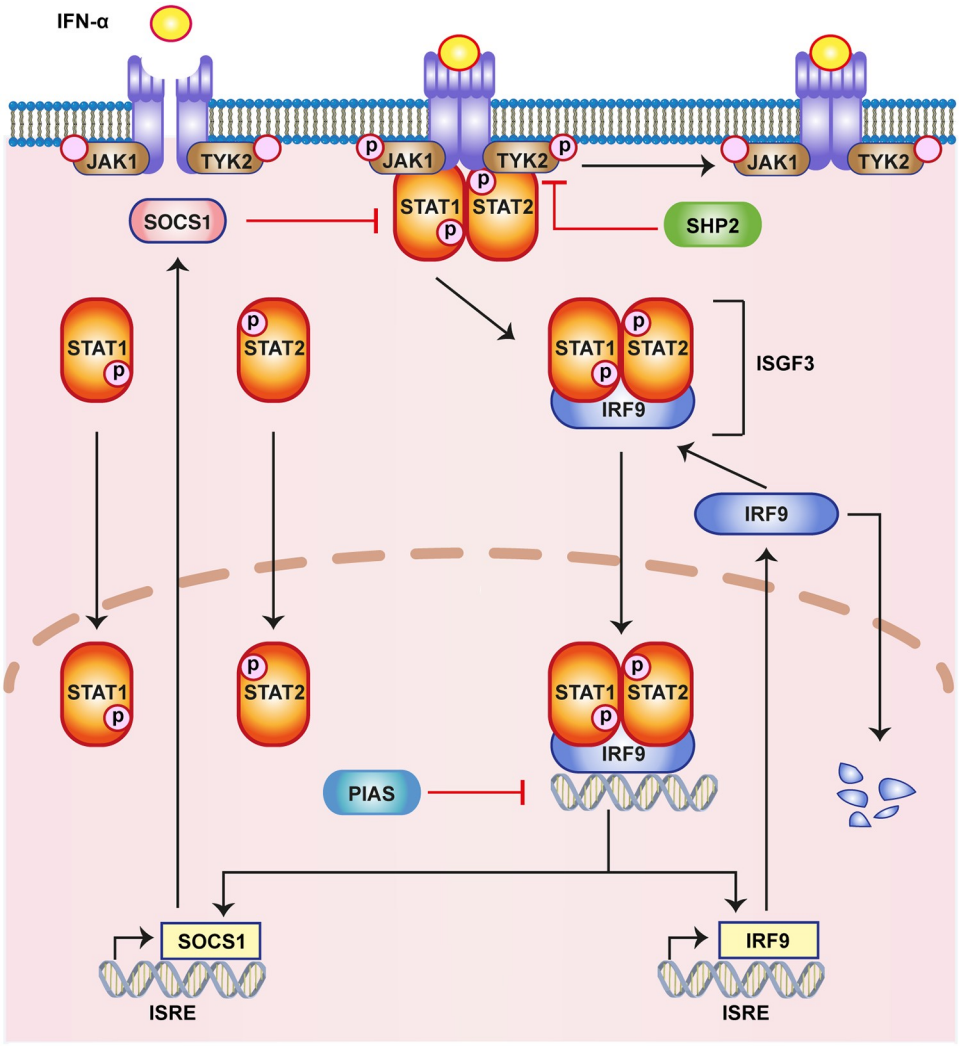

Fig 1. Illustration of the canonical JAK/STAT pathway. The key steps of the pathway in response to IFN-α are highlighted here. IFN binds to the receptor and activates JAK1 and TYK2, which subsequently activate the STATs in the cytoplasm, all by phosphorylation. The phosphorylated STATs and IRF9 form the transcription complex ISGF3, which translocates to the nucleus, where it activates hundreds of ISGs, including IRF9, Mx2 and SOCS1.

https://doi.org/10.1371/journal.pone.0209587.g001

our knowledge, thus far, this is the first study on therapeutic proteins that integrates the models of different scales in such detail. We expect such multi-scale PBPK/PD models to become of increasing importance in pharmaceutical development in the future.

Materials and methods

Software

Copasi. The cellular JAK/STAT signalling model of IFN-α was developed in Copasi [31], version 4.22, an open source software freely available at www.copasi.org.

PK-Sim. The PBPK model of IFN-α was built using the PBPK modelling software PK-Sim® (Open Systems Pharmacology suite Version 7.0 available at www.github.com).

MoBi. The PBPK protein model was established in PK-Sim (Open Systems Pharmacology suite Version 7.0). The integration of the PBPK model with the cellular JAK/STAT signalling

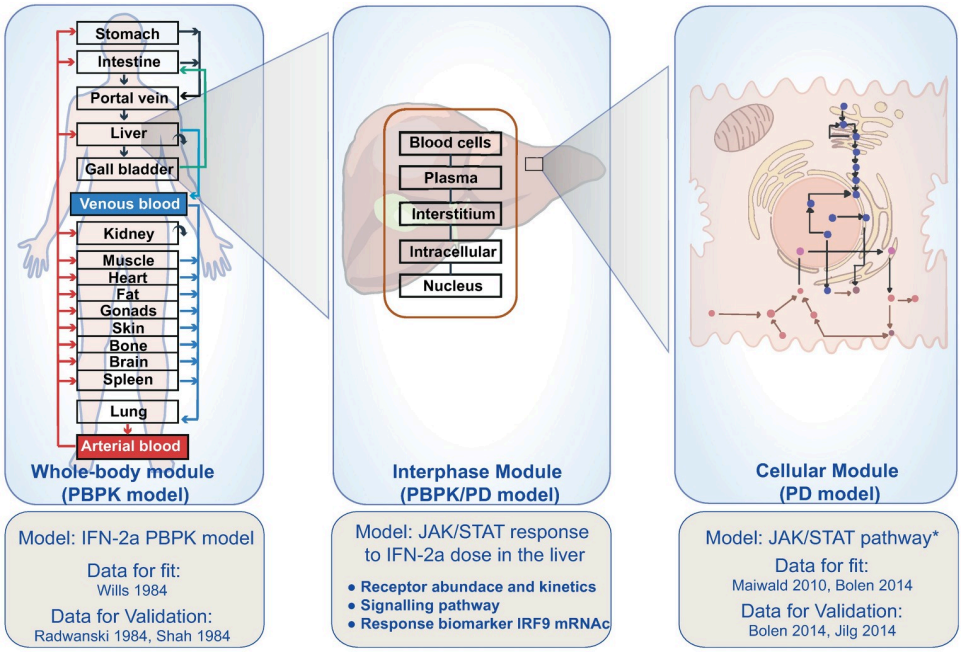

Fig 2. Integrated multi-scale PBPK/PD model. From left to right: Whole-body model (PBPK): The drug distribution is modelled using the PBPK approach at the level of the human whole-body. Integrated model (PBPK/PD): The integrated model encompasses the dose arriving from the whole-body PBPK model to the liver and the cellular model coupled to the PBPK model inside the liver. The target mediated drug disposition is modelled in the liver compartment of the PBPK model. It allows for organ level analysis after the whole-body drug distribution. Here, the biophase distribution is taken into account for large molecules. Cellular model (PD): The cellular model established by using data from hepatocytes consists of the mechanism based PD model comprising the receptor behaviour and signalling network. This model is an altered version of the model from [20] which is then coupled at the liver with the whole-body PBPK model.

https://doi.org/10.1371/journal.pone.0209587.g002

model was implemented in MoBi® (Open Systems Pharmacology suite Version 7.2 available at www.github.com).

Methods

Simulation of the models were performed using the LSODA algorithm as implemented in Copasi, as well as cvode 42 in PK Sim/MoBi. Parameter fitting was performed with the Particle Swarm and Hooke/Jeeves algorithms as implemented in Copasi for fitting intracellular dose-response behaviour and Monte Carlo/Levenberg-Marquardt implemented in the Open Systems Pharmacology suite (Matlab toolbox).

PBPK modelling. PBPK modelling allows a detailed mechanistic representation of physiological processes underlying drug ADME (ADME: absorption, distribution, metabolism and excretion) at the whole-body level. PBPK models are based on physiological information of the organism such as organ volumes or blood flows on the one hand and physicochemical properties of the drug, i.e. its molecular weight or lipophilicity on the other. In total, a PBPK model may comprise several hundreds of ordinary differential equations and a corresponding number of model parameters. However, physiological information on the organism is usually compiled in curated databases in most PBPK software parameters such that these parameters do not have to be provided by the user. In a PBPK model each organ is characterised by a blood perfusion rate or organ surface area. The various organs are linked together by arterial and venous blood compartments to allow for vascular circulation at the whole-body scale. In

addition physicochemical parameters are required to parametrise the distribution model to simulate steady state tissue concentrations as well as the corresponding passive permeation rates. Notably, the distribution of both small molecules (MW 400 g/mol) and of proteins (MW 100,000 g/mol) can be considered with PBPK modelling. The only difference in this case is an adjusted distribution model.

Results

Model set-up

The multi-scale model was obtained by establishing and merging the models as in the following steps:

1. Establishment of a PBPK model of interferon administration at the whole-body level.
2. Establishment of a revised intracellular PD model of the JAK/STAT pathway at cellular scale.
3. Integration of both models in a multiscale PBPK/PD model of IFN-α drug action.

In the following we walk through the individual steps in detail.

Establishment of a PBPK model of interferon administration at the whole-body level

For the PBPK of IFN-α weight, height and BMI of an average European individual were selected in the biometrics section of the individual. Physico-chemical information of IFN-α was obtained from the literature (S4 and S5 Tables).

The ligand-receptor interaction kinetics were represented according to the established kinetic mechanisms described in previous studies [32–34] (S2 Text). The relative protein abundance of IFNAR2 and IFNAR1 for their tissue distribution expression profiles of normal, healthy individuals was taken from an *in vivo* expression database [35]. In the PBPK model both receptors were assumed to occur in the interstitial space of the liver and the individual receptor concentrations were calculated according to the hepatocellularity of the human liver (S2 Text). For estimating the kidney clearance, elimination values by glomerular filtration rate (GFR) were inserted from the literature (S4 Table).

Intravenous administration of recombinant leukocyte IFN-α of 0.22 mg on human subjects as reported by Wills et al. (1984) [36] was used to fit the model. These data served as the basis to estimate parameters like binding affinity and internalisation to replicate the ADME profile represented therein (details in the Supplement S2 Text). Validation was done by using other datasets from literature, namely: Intravenous IFN-α doses 0.136 mg and 0.27 mg by Shah et al. (1984) [37] and 0.045 mg by Radwanski et al. (1987) [38] (see Fig 3A and 3B). The model describes these data with reasonable accuracy (see S6 Table).

PBPK models can quantify the tissue exposure to the drug. In the case of IFN-α many tissue distribution studies have been performed on animal models [39–42]. In these mouse studies, highest concentrations have been found in the spleen, liver, kidney and lungs. In this context, the concentration denotes the whole tissue concentration of IFN-α.

Tissue distribution studies are rarely possible in humans due to ethical reasons. However, the established PBPK model can give insights into the IFN-α tissue concentrations. Our simulation results suggest that the liver, spleen, lung and kidney have similar profiles as the plasma concentration (Fig 4). In particular, the concentration profile in the liver follows the dynamics of the plasma PK profile which has even been shown for higher molecular weight antibodies

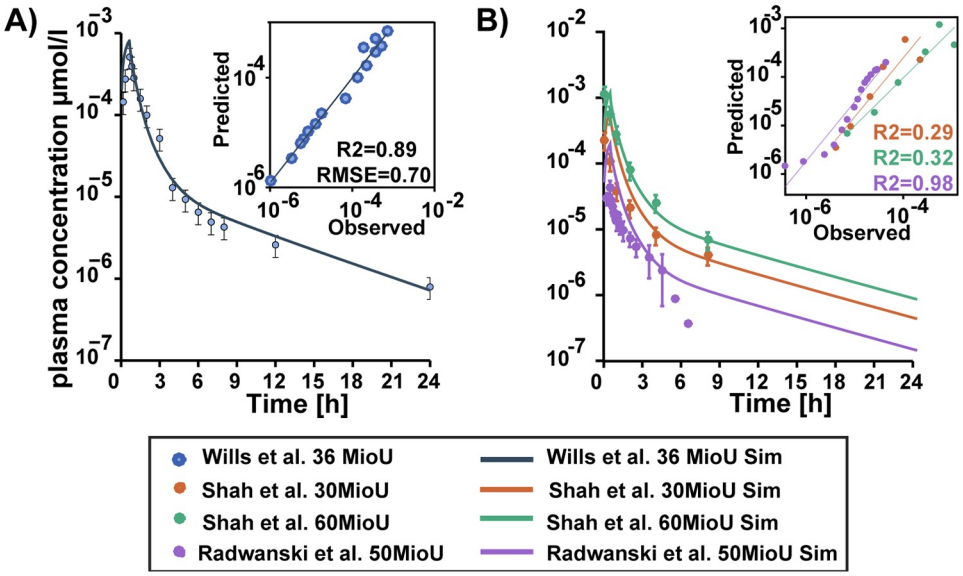

Fig 3. Physiologically based pharmacokinetic (PBPK) model fit and validation. Physiologically based pharmacokinetic (PBPK) model simulations (lines) and experimental blood plasma profile (circles) of IFN-α in humans. A) Experimental results of Wills et al. [36] and the corresponding fit. B) Model validation using blood plasma profile experiments from literature [37, 38].

https://doi.org/10.1371/journal.pone.0209587.g003

[22, 43]. On this basis, the PBPK model accurately describes the IFN-α concentration in the tissue which is of relevance for the model coupling.

Establishment of a revised intracellular PD model of the JAK/STAT pathway at cellular scale

The original intracellular model lacked details of the processes at receptor level which are a prerequisite for the model integration into the whole-body model. Therefore, we established an altered version of an IFN-α signalling model published by Maiwald et al. [20]. The original model can be retrieved from the Online Cellular Systems Modelling Database [44]. As the receptor level constitutes the interface between PBPK and intracellular model, we extended the original model by a detailed description of these receptor associated processes, using the parametrisation from the PBPK model (S1 Text, S2 and S3 Tables). This resulted in a model of 21 species and 20 reactions (S1 Table).

In this altered model, the dose response behaviour towards realistic IFN-α doses was also established. The original model was fitted to data from close to saturation doses, therefore, we used additional experimental data corresponding to responses to lower doses from the literature. In summary, this model was fitted to the data used in the original publication (Maiwald et al.(2010) [20]) which is data describing the time course of JAK, STAT, IRF9 and SOCS concentration for two hours in a population of Huh 7.5 cells in response to 2 doses: 500 and 1000 Units (U) of IFN-α (close to saturation doses). In addition and simultaneously, the following data was fitted: Data from Bolen et al.(2014)m [45] describing the dose response of IRF9 mRNAc for IFN-α doses of 10 and 100 U in a population of Huh 7.5 cells. The remaining data from Bolen et al.(2014) [45] for 500 and 2500 U doses and data from Jilg et al.(2014) [46] with dose response behaviour of IRF9 mRNAc for IFN-α doses of 15 and 30 U in a population of Huh 7.5 cells were set aside for validation purposes. In addition to the low dose responses, these data sets also capture a longer time course compared to the Maiwald et al. [20] data set.

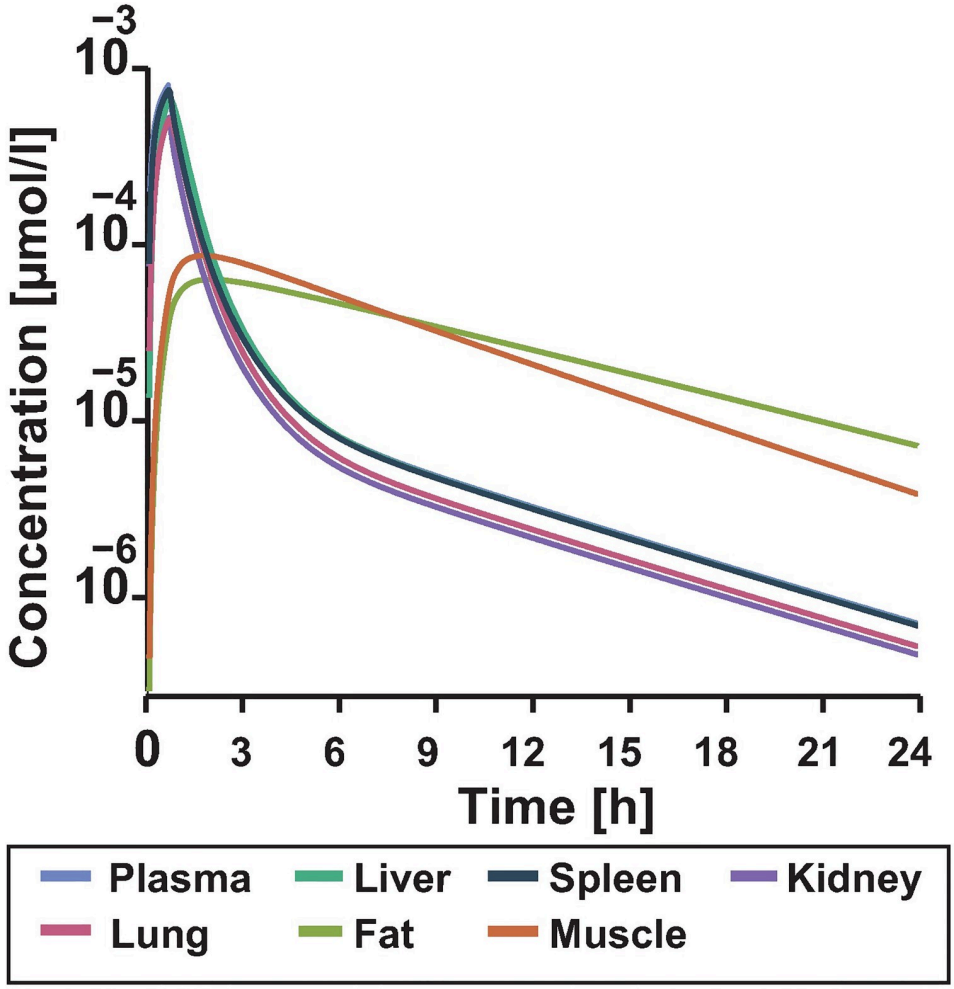

Fig 4. Simulated tissue distribution of IFN-α for the dose reported in Wills et al. (1984) [36] for 24 hours. The lines show time-course distribution of IFN-α in venous blood plasma vs. the concentration found in the tissue of the different organs.

https://doi.org/10.1371/journal.pone.0209587.g004

The fitting was achieved with the software COPASI [31] which allows the export of the models in standard SBML format [47]. The fitting procedure was repeated with different initial parameters and the ten best fits were selected for further evaluation of the model. The analysis of these fits, i.e. their parameter distributions showed that almost all parameters remained unidentifiable. Therefore, all fits were studied as a model ensemble to see if results were robust towards parameter variations as in Fig 5 and S1 Fig [48].

As seen in Fig 5 all 10 models are able to fit the experimental data almost equally well. A validation of the response in the model ensemble is done with the doses of 500U and 2500U IFN-α from Bolen et al [45] and 15U and 30U IFN-α from Jilg et al. [46] as stated previously. As the experiments originate from different publications and are in arbitrary units, they are not directly comparable with each other, but it is possible to compare a normalised relative behaviour of IRF9 mRNAc over time for different doses. This was achieved by normalising across the different doses used in each experiment to account for the fold changes. Hence, having the doses 10U, 100U, 500U and 2500U been normalised across each other, while 15U and 30U having been normalised across the two. It can be seen in Fig 6 that the dynamic behaviour of

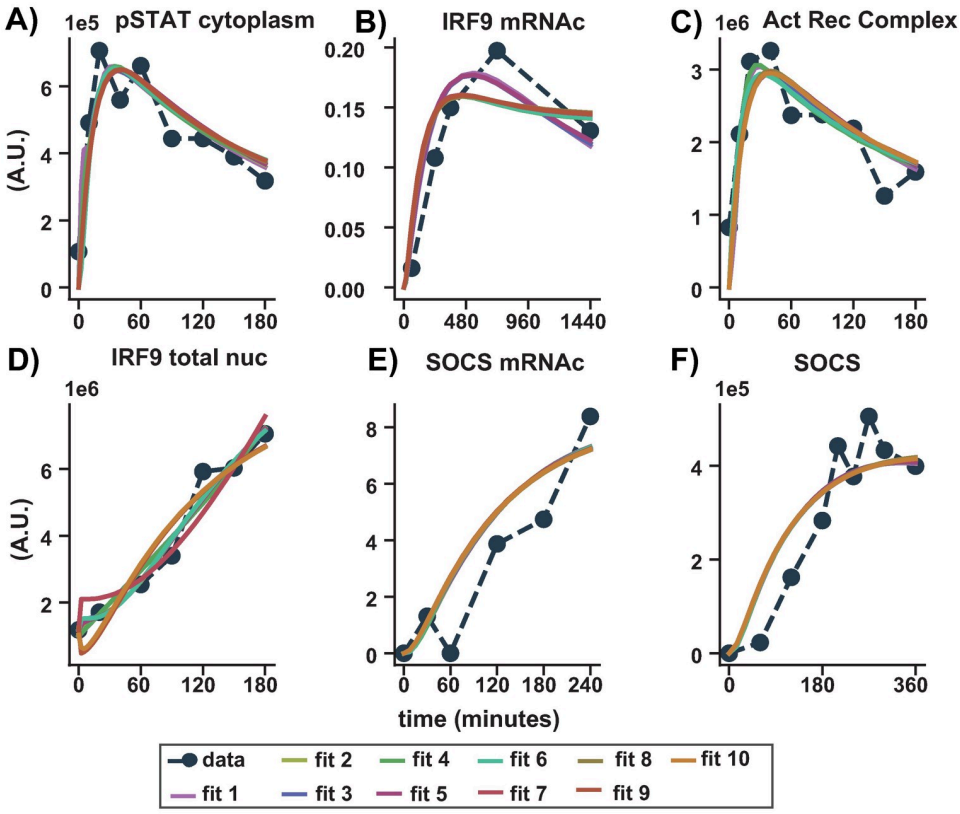

Fig 5. Fitting results of top 10 fits. Comparison between experimental time series measurements of IFN-α induced intracellular responses and computational simulations after fitting. The time after IFN-α application is given on the x-axis of each subfigure. Experimentally determined levels of the measured proteins are presented as filled dots and dashed lines (A) pSTAT, C) pJAK (Act Rec Complex), D) IRF9 total in the nucleus, E) SOCS mRNAc and F) SOCS protein measured by quantitative-immunoblotting in Huh 7.5 cells after stimulation with 500 U IFN-α as in Maiwald et al. [20]. B) dynamic expression of IRF9 mRNA fold change in Huh 7 cells for 10 U IFN-α as shown in Bolen et al. [45]. Computational fit shown as solid lines. Fits to full 20 dataset are shown in the supplementary S2 Fig.

https://doi.org/10.1371/journal.pone.0209587.g005

the model ensemble for 500U and 2500U quantifies the time course data dynamics quite well, although for 2500U the peak concentration is underestimated ((A) and (B)). In Fig 6C) and 6D), the model ensemble overestimates the peak of the time course, but estimates the dynamic behaviour for 15U quite well. However, it also underestimates the response for 30U. It should be noted that in the latter data set a different subtype of interferon was used and the general experimental set up differed. The model shows saturation behaviour already for 100U (hollow circles) which is close to the experimentally estimated saturation dose (between 50U to 100U) (Fig 6E)) as can be seen in the literature (as listed in S3 Fig).

Integration of both models in a multiscale PBPK/PD model of IFN-α drug action

The intracellular pathway model was next integrated into the whole-body PBPK model such that, structurally, the intracellular signalling was assumed to happen in the liver compartment only. For this purpose, the intracellular model which was developed using the software COPASI had to be manually transferred to MoBi®. To ensure the correctness of the model transfer, we tested for the consistency in two ways. First, the agreement between simulations of the cellular model in both software tools was verified. Second, after the integration simulations

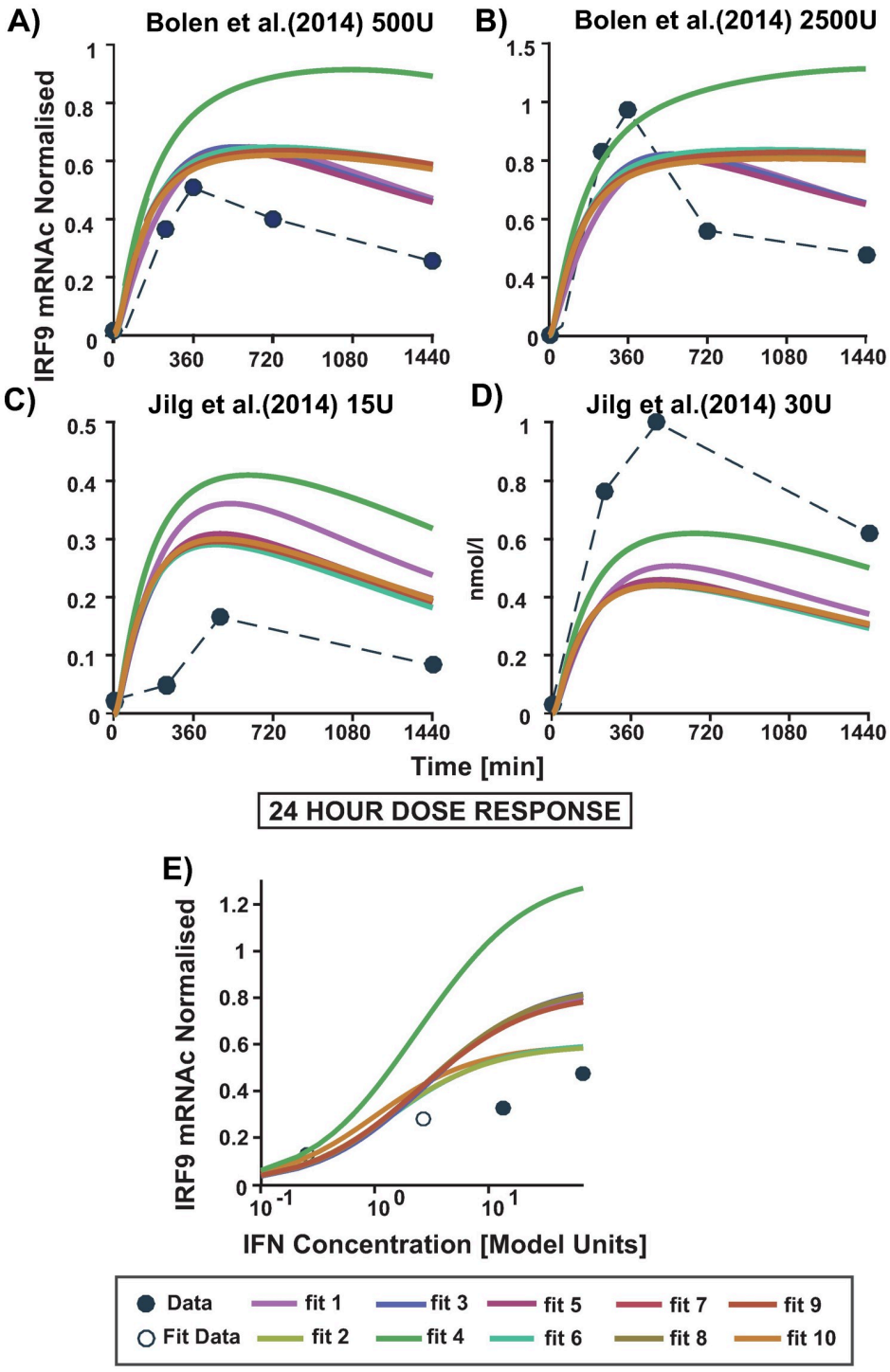

Fig 6. The validation of the dose response for the top ten fits. In A-D) the time course of the 4 experimental doses (circles) is plotted together with the calculated simulation of the top ten models (solid lines). The different doses taken in account are, in A) 500 U and B) 2500U of IFN-α as published by Bolen et al. [45]. C) 15U and D) 30U of IFN-α as in Jilg et al. [46]. In the panel E) and F) the 24 hour dose response (DR) curve is shown for all the data obtained from the literature where E) has DR simulation for 24th hours representing data from Bolen et al. [45] for 10U, 100U, 500U and 2500U.

https://doi.org/10.1371/journal.pone.0209587.g006

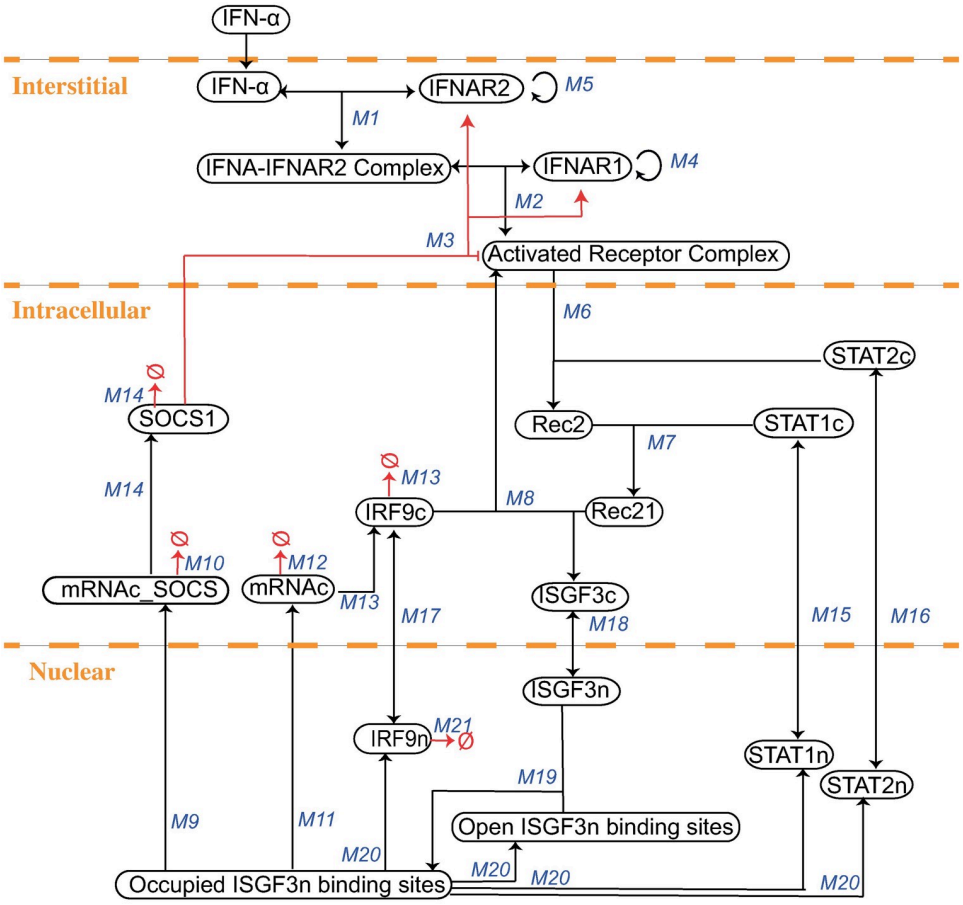

Fig 7. The model schema of the mechanistically based PBPK/PD model details at the liver. The IFN-α is cleared via the binding to the respective receptors in the liver. The binding of IFN-α to the IFNAR2 and IFNAR1 takes place in the interstitium of the liver (M1-M5), hence activating the JAK/STAT pathway leading to the activation of mRNAc of the response protein IRF9 in the intracellular part of the liver (M6-M14). The reactions in the interstitim constitute the interaction between the PBPK and the intracellular model. Parameterisation is derived from the PBPK model.

https://doi.org/10.1371/journal.pone.0209587.g007

with the detailed PBPK/PD model were compared with results of the cellular model for similarity. To this end, the reactions which connect the pharmacokinetic model with the intracellular model were defined in the interstitial compartment of the whole-body model (see Fig 7) and concentrations in interstitial compartment of the PBPK model were set equal to the *in vitro* concentrations. Additionally, the administration of IFN-α in the PBPK model was neglected and set to zero to validate the congruence.

Analysis of the integrated model

The integrated PBPK/PD model of IFN-α model allows the simultaneous description of IFN-α pharmacokinetics at the whole-body level following intravenous administration and the resulting pharmacodynamic response in the JAK/STAT signalling cascade in an *in vivo* context. The pharmacokinetic behaviour of therapeutic proteins is often influenced by binding to a specific target, i.e. for example an antigen receptor. The model allows quantification of the IFN-α receptor induced intracellular PD response and estimates the actual amount of IFN-α at the site of action, namely the liver.

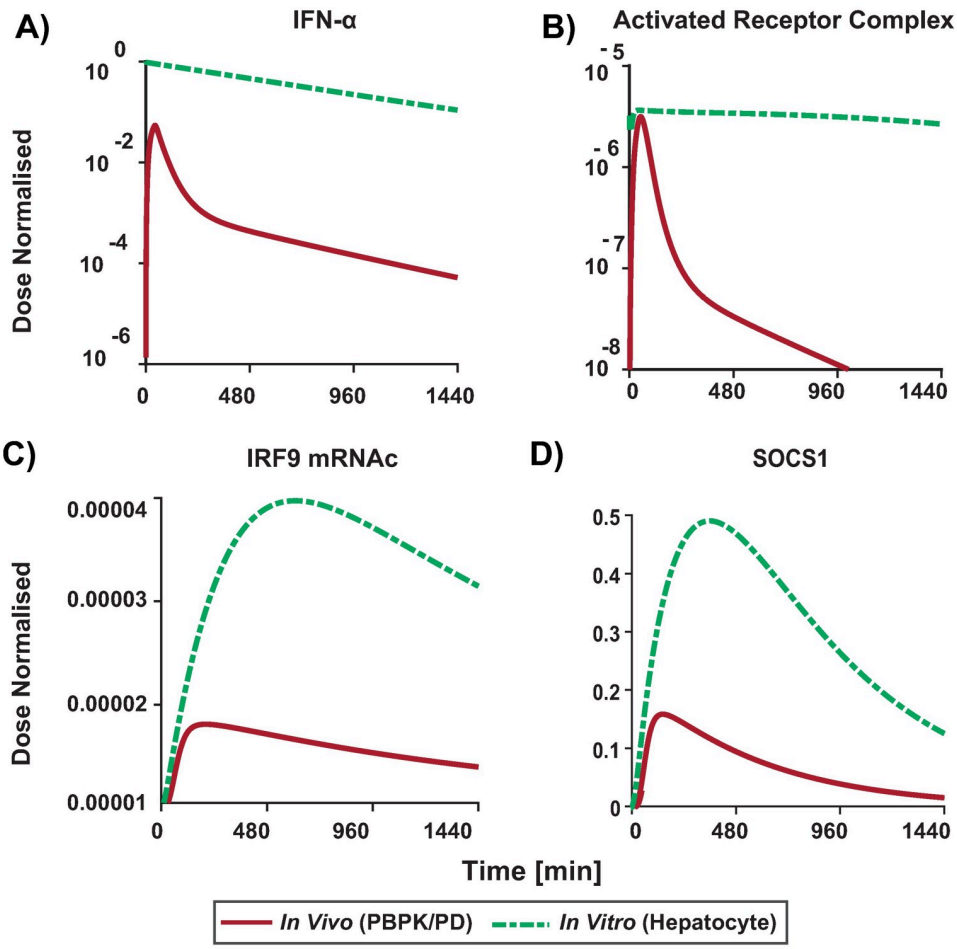

Fig 8. Relative difference in signalling dynamics in the *in vivo* (PBPK/PD) response (to 36U typically administered dose) vs. the *in vitro* (hepatocyte) response (to 500U as typically used in experimental setups). PBPK/PD model (red lines), hepatocyte culture simulation (green lines). Simulation of concentration time profiles in human and in human cell lines of A) the non-linear IFN-α, B) activated receptor complex C) IRF9 mRNAc and D) SOCS1 activated downstream in the models.

https://doi.org/10.1371/journal.pone.0209587.g008

Next, we simulated the injection of an IFN-α dose (36 U) as in [36] with the fully integrated model and followed the behaviour of the intracellular response. In particular, we compared the constant *in vitro* experiment concentration (500 U [20, 45, 49, 50]) to a realistic *in vivo* situation following an i.v. injection of 36 U of IFN-α [36] Fig 8. We found that the *in vivo* scenario lead to a C_{max} of 0.7 nmol/l while in the *in vitro* experiments a C_{max} of 13 nmol/l is reached. Obviously, it is to be expected that there are differences in the dynamics of the signalling pattern between *in vivo* and *in vitro* situations and doses (Fig 8B–8D). For example the onset of the *in vitro* response is slightly faster than the *in vivo* response although the C_{max} is reached faster *in vivo*. Interestingly, our simulations suggest the same trend when using the administered dose (C_{max} of 0.7 nmol/l) in the *in vitro* settings (S6 Fig).

The integrated PBPK/PD model allows further mechanistic insights in the dose-response correlation. Our simulation results indicate that the *in vitro* dose are typically too high to be comparable with the *in vivo* situation. However, being close to receptor saturation (Fig 9C) a 18x higher dose (36 U vs 500 U), only results in a 4 fold difference in response, i.e. IRF9 mRNAc (see Fig 9D).

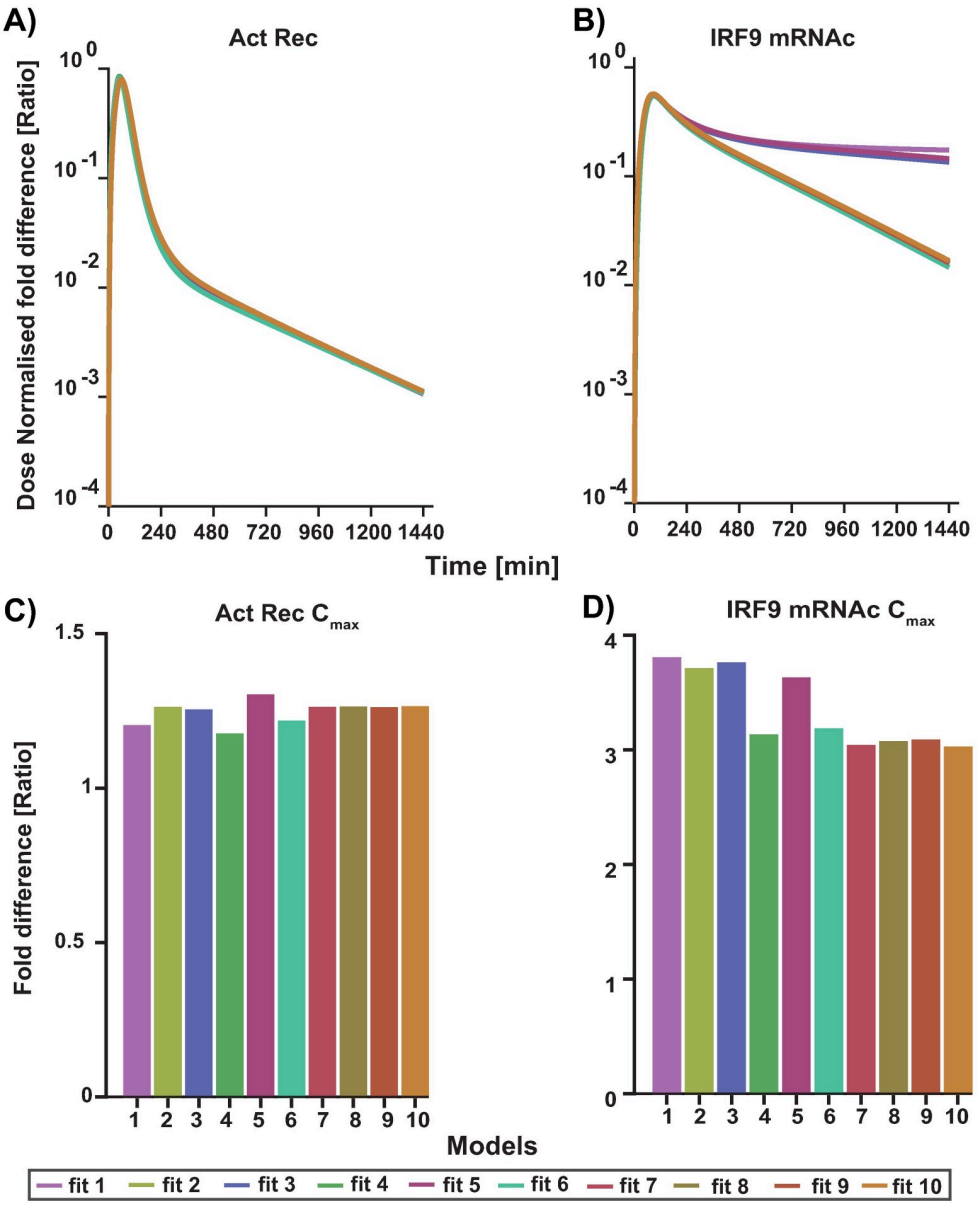

Fig 9. Comparison of cellular signalling responding to typical experimental vs *in vivo* stimulation with IFN-α. Intracellular signalling was modelled in response to a constant dose of 500U (as typically used *in vitro*) in comparison to the calculated PBPK profile resulting from a typical dose of 36U. Fold difference is plotted of A) Activated receptor complex and B) IRF9 mRNAc simulation (solid lines) concentration time profile for the top ten models. C) The calculated fold difference C_{max} achieved for activated receptor complex (Act Rec) (bars for each model respectively) and D) fold difference in the C_{max} of IRF9 mRNAc.

https://doi.org/10.1371/journal.pone.0209587.g009

In order to have a comparison of the T_{max} achieved *in vivo* vs *in vitro*, we simulated a constant *in vitro* dose of 0.7 nmol/l (36 U dose) which corresponds to the C_{max} concentration arriving at the liver in our simulation. Because of the lack of drug clearance the *in vitro* behaviour shows a stronger and more sustained response than *in vivo* (S4, S5 and S6 Figs). It is however, interesting to note that despite the numerical differences in dose and cellular response, the shape of the *in vivo* and the *in vitro* PD profile are rather similar (Fig 8C and 8D). In particular, it is worthwhile mentioning that the cellular response is only transient due to negative

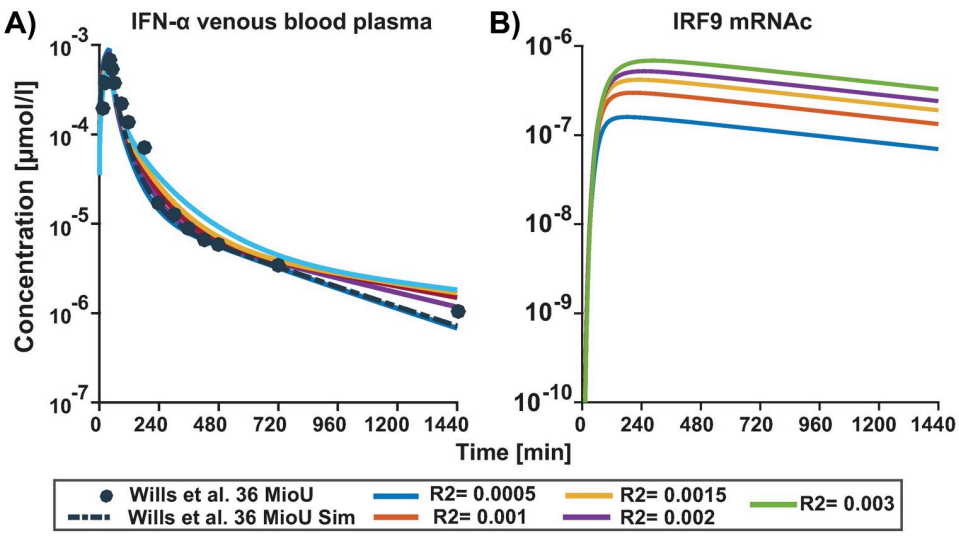

Fig 10. Parameter scan for the initial concentration of IFNA Receptor2. PBPK/PD simulation (lines) of concentration time profile for A) IFN-α in venous blood plasma and the experimental blood plasma profile (solid circles) of IFN-α in humans. B) IRF9 mRNAc response to different initial concentrations of IFN-α Receptor2 that are 0.0005, 0.002, 0.003, 0.0015 and 0.001 $\mu mol/l$. The reference concentration in the initial simulation (dashed black line) for Receptor2 was 0.5 $\mu mol/l$.

https://doi.org/10.1371/journal.pone.0209587.g010

feedback loops in the JAK/STAT signalling cascade. However, the time scales on which the cellular response reaches its peak is very different in the *in vivo* and the *in vitro* situation, respectively, as reflected by the different T_{max} values.

Variations in physiological parameters will strongly influence the results. For example receptor ligand binding is one of the essential steps that determines the clearance of IFN-α in liver. In our multi-scale PBPK/PD model the influence of this process can be easily assessed by varying the concentrations of IFN-α R2 via a parameter scan. Hence, we investigated the impact of receptor abundance and receptor ligand binding on the responses which are not only essential for IFN-α clearance by the liver but also will be one of the accountable component of patient variability. We mimicked differences in both receptor abundancy as well as receptor binding (since in the model both parameters will have a correlated effect being part of mass action kinetics). The parameter scan of different concentrations of IFN-α receptor 2 (R2) leads to little difference in the plasma ADME of IFN-α (Fig 10A) but noticeable difference in response mRNAc concentration profiles (Fig 10B) highlighting the impact of ligand binding to the receptor on the clearance of IFN-α at target site (liver) and the notable response difference for the same when considering IRF9 mRNAc as a functional endpoint.

Discussion

This work presents a multi-scale, mechanistic PBPK/PD model of IFN-α drug action. It integrates the whole-body distribution model (data from [36]) with JAK/STAT signalling. In this work we apply a quantitative systems pharmacology approach, to investigate the temporal relationships between IFN-α pharmacokinetics and the downstream pharmacodynamic responses in the JAK/STAT pathway. To this end, we developed a multi-scale PBPK/PD model which simultaneously describes two levels of biological organisation: IFN-α distribution at the organism scale as well as the resulting cellular response in the JAK/STAT pathway. Taken together this model integration allows the establishment of dose-effect relationships for IFN-α at the whole-body level. The resulting model compares *in vitro* drug-responses to therapeutic

outcomes in an *in vivo* situation amongst others. The model highlights the fourfold IRF9 mRNAc response difference when comparing typical *in vitro* dose (S3 Fig, see 500U predominantly used in most experiments) to *in vivo* dose of 36U IFN-α.

In the past, genome scale network models have been integrated in PBPK models [51, 52]. Also PBPK models have been coupled with simplistic or abstract dynamic cellular network models [53–55]. Semi-mechanistic PK/PD models were built using monkey, mouse and human data [56–59]. Additionally, on the macro-scale, analysis of different routes of injections on IFN-α pharmacokinetic is addressed by statistical modelling (a.k.a mixed effect models) [60–63]. Moreover, two compartment PK/PD models on patient populations have been reported in the literature [36, 38, 64–66]. The multi-scale PBPK/PD model presented here is a unique example of linking a detailed cellular signalling model to a whole-body PBPK model using the case of therapeutic protein. Detailed models have the advantage that they allow a direct mechanistic mapping of experimental data and modelling results and therefore the prediction of potential interference with specific points in the system.

in vitro assays are routinely used in preclinical drug development as well as in systems biology research in order to understand a cellular response. Doubtlessly, they have been very successful in many respects [67–69]. The results of the PBPK/PD model approach can help to improve the *in vitro* assay design through reverse dosimetry such that the IFN-α dose of actual physiological relevance are used in the experiments [70]. As described above, the intracellular signalling is four fold reduced in physiological conditions and displays different dynamics due to *in vivo* drug elimination [71–73].

This is of particular relevance since *in vitro* concentrations are frequently chosen at high and saturating levels like in the case of IFN-α where the dose of 500 U is normally used for experiments. This trigger is apparently not reflecting the natural, physiological situation nor the one during clinical usage. We are aware that our intracellular models have been based on such studies and it can be questioned, how close the data gained from cell lines in culture is representing the actual behaviour of cells in a tissue and an *in vivo* environment. However, in [20] there has been at least a comparison between the cell line used and primary hepatocytes showing that the results of the cell lines were very similar both quantitatively and dynamically as compared to primary cells. Again, isolated primary cells are not consistently behaving as they would in their physiological context. So, it is possible that the actual cellular response might be stronger than what we estimate here in this study, e.g. due to paracrine signalling in response to IFN-α. However, in the absence of methodology that follows IFN-α signalling *in vivo* in a time-dependent manner, this work quantifies the differences between *in vivo* and *in vitro* scenarios. Thus, approaches like this model can contribute to techniques like *in vitro-in vivo* extrapolation. The results of the PBPK/PD model approach can help to improve the *in vitro* assay design so that IFN-α of actual physiological levels and timings are used. Integration of the pharmacokinetic behaviour with the intracellular signalling is profoundly different from having the separately calculated amount of IFN-α in the liver as an administrated dose to the hepatocyte (virtual compartment in the model) and calculating the corresponding response. In the integrated model, both processes occur simultaneously and any time-dependent change in the availability of the drug at the site of action immediately influences the cellular behaviour.

As tissue distribution studies in humans are clinically infeasible, PBPK/PD models as the one presented in this study can be used to quantify tissue exposure and can be compared with animal model experiments. As an add-on, such a model helps to quantify differences between animal studies and human patients. Since target mediated disposition was found to play a major role in the therapeutic efficiency of IFN-α treatments, it is furthermore conceivable that PBPK/PD models are individualised through different quantitative phenotypes of antigen presenting individuals.

Another point to be aware of is that the dosages and concentrations of IFN-α are given in biological units of its activity. This magnitude is derived from the established activity of a reference standard. These standards however often differ in each study. Thus, it is often difficult to compare doses and serum concentrations quantitatively. Moreover, many studies in the literature do not publish the established activity unit conversions hence leading to constraints for quantitative models.

It should be noted that for the cellular scale a lot of experimental data were available for this work, most of these measurements were from short time scales ranging between 2-6 hours. However, for long-term behaviour much less data is available and therefore the model has limits to quantify the long-term behaviour. However, the important intracellular observations, namely peak amplitude and the speed of activation occur within the short time for which we had a high degree of confidence. For some proteins we could rely on quantitatively calibrated concentration profiles. However, for proteins which are measured without calibrator and only given in relative arbitrary units in the experimental time series, the model is only able to quantify relative changes. This is especially true for the amount of mRNAs simulated. Therefore, we normalised the data and do not work with absolute amounts for these species. In addition, the data used for validation is from experiments that use other subtypes of IFN-α. Using different subtype only for the validation ensures that the calibration of the model is not changed as the fitting was done by using only one subtype of IFN-α (IFN-α 2a). Although, the subtypes may have differences in their specific and kinetic activity, it seems that the qualitative trends in the induced cellular responses are quite similar among the IFN-α subtypes.

The PBPK/PD model of IFN-α also allowed the derivation of the concentration-effect relationship between IFN-α and its response on the functional biomarker IRF9 mRNAc. The model suggests that the saturated response of IRF9 mRNAc is attained at lower IFN-α administered dose in comparison to *in vitro* experiments.

A significant observation is that in classical PK/PD models one only infers the dose with simplistic models in combination with plasma concentration levels which are not comparable to the integration of a detailed signalling cascade as undertaken here. This may be in particular true for biologics like IFN-α as they are produced by most cells of our body and function in both autocrine and paracrine manner. Hence, such a systemic effect at the whole-body level may only be possible to describe with a multi-scale PBPK/PD modelling approach. Finally, we would like to stress that the described pipeline could be used for any drug eliciting intracellular responses and is by no means restricted to IFN-α signalling. Patient specific data can be integrated at the level of protein abundancies, e.g. for the receptors. In the end, for an at least semi-automated set-up of such integrated multi-scale models it would be important to specify a common standard for model exchange between the cellular and pharmacokinetic models.

Conclusion

In this work we established a multi-scale PBPK/PD model for IFN-α combining the pharmacokinetic behaviour of the therapeutic protein after administration to a human and the intracellular signalling elicited by the administered dose. We observed that intracellular responses in physiological conditions is reduced compared with the one reported in cell cultures, albeit only about four fold.

The presented multi-scale PBPK/PD model supports a mechanistic understanding of how a cellular system responds to drug administration. This is of particular relevance, since many new drug therapies are using protein therapies and at the same time envisage personalised treatment regimes for individual patients. This model exemplifies that in the case of therapeutic proteins (biologics), establishing such in-detail models strengthen insights of the dose effect

relationships. Due to the ubiquitous presence of such proteins in our bodies, small tweaks at the physiological level can lead to visibly different responses in the cellular pathway. A mechanistic understanding of the complex interplay of a patient's physiology and mechanistic pharmacodynamics is of primary importance to account for the complex interplay of feedbacks and the biomarkers established to study that. Notably, the presented workflow is generic and therefore not limited to therapeutic proteins [74]. Last but not least, this work highlights the major dynamic dose-effect relationship differences between in physiology vs. cell culture conditions and helps to shed light on the missing aspects and knowledge of the same.

Supporting information

S1 Text. Cellular model description.
(PDF)

S2 Text. Pharmacokinetic model description.
(PDF)

S1 Table. Reaction list.
(PDF)

S2 Table. Description of the kinetic parameter values.
(PDF)

S3 Table. k_D values found in the literature.
(PDF)

S4 Table. Values of the literature parameters for the PBPK model of IFN-α used in this study.
(PDF)

S5 Table. Volumes of the liver compartments.
(PDF)

S6 Table. C_{max} and AUC values.
(PDF)

S1 Fig. The full scheme of kinetic model of the IFN-α signalling pathway.
(TIF)

S2 Fig. The top ten fits. The top ten fits obtained from the fitting process for 20 datasets is depicted. In the figure the time course profile for A) pStat cytoplasm in response to 500 U B) pSTAT nucleus in response to 500 U C) pSTAT cytoplasm with overexpression of IRF9 protein D) pSTAT nucleus with overexpression of IRF9 protein E) pStat cytoplasm in response to 500 U (second replicate) F) pSTAT nucleus in response to 500U (second replicate) G) IRF9 mRNAc in response to 10U from Bolen et al. [45] H) IRF9 mRNAc in response to 100U from Bolen et al. [45] I) pSTAT total in nucleus in response to 500 U J) pSTAT total in cytoplasm in response to 500U K) pSTAT total in nucleus in response to 1000 U L) pSTAT total in cytoplasm in response to 1000U M) pJak in response to 500U (Activated receptor complex)) N) pSTAT total in nucleus O) IRF9 protein total in nucleus P) mrna socs in response to 500U Q) mrna socs with overexpression of IRF9 protein R) pSTAT total in nucleus in response to 500U S) SOCS protein with overexpression of IRF9 protein T) SOCS protein in response to 500U.
(TIF)

S3 Fig. IFN-α dose response data on cell lines as found in literature.
(TIF)

S4 Fig. IRF9 mRNAc T_{max}. This table shows the difference in time scale of achieving the maximum concentrations when the IFN-α constant dose is simulated as the *in vivo* dose (0.7 nmol/l instead of 13 nmol/l) in the top ten models for PBPK/PD model (*in vivo*) in the liver and in the hepatocyte (*in vitro*) conditions is depicted.
(TIF)

S5 Fig. Simulation of the hepatocyte *in vitro* model with the *in vivo* dose (C_{max} 0.7 nmol/l). Relative fold difference of IRF9 mRNAc T_{max} calculated by simulating the typical administered dose of 36U IFN-α (C_{max} 0.7 nmol/l) for PBPK/PD and *in vitro* hepatocyte model.
(TIF)

S6 Fig. Simulation of IFN-α response comparing a constant (green) and a dynamic (red) dose as seen *in vivo* for identical C_{max} of 0.7 nmol/l. Temporal dynamics of A)IFN-α B) Activated Receptor Complex C) IRF9 mRNAc D) SOCS.
(TIF)

Acknowledgments

The author wishes to thank Christopher R. Bolen, Michael D. Robek and Steven H. Kleinstein from Yale University for kindly providing the data for IRF9 in Huh 7 and primary human hepatocytes from their publication. Luis Aguilera for fruitful discussions regarding the work.

Author Contributions

Conceptualization: Lars Küpfer, Ursula Kummer.

Funding acquisition: Ursula Kummer.

Investigation: Priyata Kalra, Julian Brandl, Lars Küpfer.

Methodology: Priyata Kalra, Julian Brandl, Thomas Gaub, Christoph Niederalt, Sven Sahle.

Software: Priyata Kalra, Thomas Gaub, Christoph Niederalt.

Supervision: Jörg Lippert, Sven Sahle, Lars Küpfer, Ursula Kummer.

Writing – original draft: Priyata Kalra, Lars Küpfer, Ursula Kummer.

Writing – review & editing: Priyata Kalra, Julian Brandl, Christoph Niederalt, Jörg Lippert, Sven Sahle, Lars Küpfer, Ursula Kummer.

References

1. Di Bisceglie AM. Hepatitis C. Lancet. 1998; 351(9099):351–5. https://doi.org/10.1016/S0140-6736(97)07361-3 PMID: 9652633
2. Alter MJ, Margolis HS, Krawczynski K, Judson FN, Mares A, Alexander WJ, et al. The natural history of community-acquired hepatitis C in the United States. The Sentinel Counties Chronic non-A, non-B Hepatitis Study Team. N Engl J Med. 1992; 327(27):1899–905. https://doi.org/10.1056/NEJM199212313272702 PMID: 1280771
3. Friedman RM. Clinical uses of interferons; 2008.
4. Hoofnagle JH, Seeff LB. Peginterferon and ribavirin for chronic hepatitis C. The New England journal of medicine. 2006; 355(23):2444–2451. https://doi.org/10.1056/NEJMct061675 PMID: 17151366
5. Fried MW, Shiffman ML, Reddy KR, Smith C, Marinos G, Gonçales FL, et al. Peginterferon alfa-2a plus ribavirin for chronic hepatitis C virus infection. The New England journal of medicine. 2002; 347(13):975–82. https://doi.org/10.1056/NEJMoa020047 PMID: 12324553

6. Di Bisceglie AM, Shiffman ML, Everson GT, Lindsay KL, Everhart JE, Wright EC, et al. Prolonged therapy of advanced chronic hepatitis C with low-dose peginterferon. The New England journal of medicine. 2008; 359(23):2429–41. https://doi.org/10.1056/NEJMoa0707615 PMID: 19052125
7. Jacobson IM, McHutchison JG, Dusheiko G, Di Bisceglie AM, Reddy KR, Bzowej NH, et al. Telaprevir for previously untreated chronic hepatitis C virus infection. The New England journal of medicine. 2011; 364(25):2405–16. https://doi.org/10.1056/NEJMoa1012912 PMID: 21696307
8. Poordad F, McCone J, Bacon BR, Bruno S, Manns MP, Sulkowski MS, et al. Boceprevir for untreated chronic HCV genotype 1 infection. The New England journal of medicine. 2011; 364(13):1195–206. https://doi.org/10.1056/NEJMoa1010494 PMID: 21449783
9. Lavanchy D. The global burden of hepatitis C. In: Liver International. vol. 29; 2009. p. 74–81.
10. Gutterman JU. Cytokine therapeutics: lessons from interferon alpha. Proceedings of the National Academy of Sciences of the United States of America. 1994; 91(4):1198–205. https://doi.org/10.1073/pnas.91.4.1198 PMID: 8108387
11. Heintges T, Mohr L, Hensel F, Petry W, Borchard F, Haussinger D, et al. Value of liver biopsy prior to interferon therapy for chronic viral hepatitis. Dig Dis Sci. 1998; 43(7):1562–1565. https://doi.org/10.1023/A:1018827201670 PMID: 9690395
12. Trifan A, Stanciu C. Checkmate to liver biopsy in chronic hepatitis C? World Journal of Gastroenterology. 2012; 18(39):5514–5520. http://dx.doi.org/10.3748/wjg.v18.i39.5514 PMID: 23112543
13. Samuel CE. Antiviral Actions of Interferons. Clinical Microbiology Reviews. 2001; 14(4):778–809. https://doi.org/10.1128/CMR.14.4.778-809.2001 PMID: 11585785
14. Chen L, Borozan I, Feld J, Sun J, Tannis LL, Coltescu C, et al. Hepatic gene expression discriminates responders and nonresponders in treatment of chronic hepatitis C viral infection. Gastroenterology. 2005; 128(5):1437–44. https://doi.org/10.1053/j.gastro.2005.01.059 PMID: 15887125
15. Sarasin-Filipowicz M, Oakeley EJ, Duong FH, Christen V, Terracciano L, Filipowicz W, et al. Interferon signaling and treatment outcome in chronic hepatitis C. Proc Natl Acad Sci U S A. 2008; 105(19):7034–9. https://doi.org/10.1073/pnas.0707882105 PMID: 18467494
16. Witthoft T. Review of consensus interferon in the treatment of chronic hepatitis C. Biologics. 2008; 2(4):635–643. PMID: 19707444
17. Chen L, Borozan I, Sun J, Guindi M, Fischer S, Feld J, et al. Cell-type specific gene expression signature in liver underlies response to interferon therapy in chronic hepatitis C infection. Gastroenterology. 2010; 138(3):1123–1133. https://doi.org/10.1053/j.gastro.2009.10.046 PMID: 19900446
18. Wu HL, Hsiao TH, Chen PJ, Wong SH, Kao JH, Chen DS, et al. Liver Gene Expression Profiles Correlate with Virus Infection and Response to Interferon Therapy in Chronic Hepatitis B Patients. Sci Rep. 2016; 6:31349. https://doi.org/10.1038/srep31349 PMID: 27546197
19. Danhof M. Systems pharmacology—Towards the modeling of network interactions. European Journal of Pharmaceutical Sciences. 2016; 94:4–14. https://doi.org/10.1016/j.ejps.2016.04.027 PMID: 27131606
20. Maiwald T, Schneider A, Busch H, Sahle S, Gretz N, Weiss TS, et al. Combining theoretical analysis and experimental data generation reveals IRF9 as a crucial factor for accelerating *IFN–α*-induced early antiviral signalling. FEBS Journal. 2010; 277(22):4741–4754. https://doi.org/10.1111/j.1742-4658.2010.07880.x PMID: 20964804
21. Kuepfer L, Niederalt C, Wendl T, Schlender JF, Willmann S, Lippert J, et al. Applied Concepts in PBPK Modeling: How to Build a PBPK/PD Model. CPT: Pharmacometrics & Systems Pharmacology. 2016; 5(10):516–531.
22. Niederalt C, Kuepfer L, Solodenko J, Eissing T, Siegmund HU, Block M, et al. A generic whole body physiologically based pharmacokinetic model for therapeutic proteins in PK-Sim. Journal of Pharmacokinetics and Pharmacodynamics. 2018; 45(2):235–257. https://doi.org/10.1007/s10928-017-9559-4 PMID: 29234936
23. Goldstein B, Faeder JR, Hlavacek WS. Mathematical and computational models of immune-receptor signalling. Nature reviews Immunology. 2004; 4(6):445–456. https://doi.org/10.1038/nri1374 PMID: 15173833
24. Yamada S, Shiono S, Joo A, Yoshimura A. Control mechanism of JAK/STAT signal transduction pathway. FEBS Letters. 2003; 534(13):190–196. http://dx.doi.org/10.1016/S0014-5793(02)03842-5 PMID: 12527385
25. Sharma V, Compagnoni A. Computational and Mathematical Models of the JAK-STAT Signal Transduction Pathway. In: Proceedings of the 2013 Summer Computer Simulation Conference. SCSC'13. Vista, CA: Society for Modeling & Simulation International; 2013. p. 15:1–15:8. Available from: http://dl.acm.org/citation.cfm?id=2557696.2557714.

26. Vera J, Rateitschak K, Lange F, Kossow C, Wolkenhauer O, Jaster R. Systems biology of JAK-STAT signalling in human malignancies. Progress in Biophysics and Molecular Biology. 2011; 106(2):426–434. http://dx.doi.org/10.1016/j.pbiomolbio.2011.06.013 PMID: 21762720

27. Gambin A, Charzynska A, Ellert-Miklaszewska A, Rybinski M. Computational models of the JAK1/2-STAT1 signaling. JAK-STAT. 2013; 2(3):e24672. https://doi.org/10.4161/jkst.24672 PMID: 24069559

28. Rand U, Rinas M, Schwerk J, Nöhren G, Linnes M, Kröger A, et al. Multi-layered stochasticity and paracrine signal propagation shape the type-I interferon response. Molecular Systems Biology. 2012; 8(1). https://doi.org/10.1038/msb.2012.17 PMID: 22617958

29. Stark GR, D JE Jr. The JAK-STAT Pathway at Twenty. Immunity. 2012; 36(4):503–514. http://dx.doi.org/10.1016/j.immuni.2012.03.013 PMID: 22520844

30. Heneghan AF, Pierre JF, Kudsk KA. JAK-STAT and intestinal mucosal immunology. JAK-STAT. 2013; 2(4):e25530. https://doi.org/10.4161/jkst.25530 PMID: 24416649

31. Hoops S, Sahle S, Gauges R, Lee C, Pahle J, Simus N, et al. COPASI—a COmplex PAthway SImulator. Bioinformatics. 2006; 22(24):3067–3074. https://doi.org/10.1093/bioinformatics/btl485 PMID: 17032683

32. Lamken P, Lata S, Gavutis M, Piehler J. Ligand-induced Assembling of the Type I Interferon Receptor on Supported Lipid Bilayers. Journal of Molecular Biology. 2004; 341(1):303–318. http://dx.doi.org/10.1016/j.jmb.2004.05.059 PMID: 15312780

33. Gavutis M, Lata S, Lamken P, Müller P, Piehler J. Lateral Ligand-Receptor Interactions on Membranes Probed by Simultaneous Fluorescence-Interference Detection. Biophysical Journal. 2005; 88(6):4289–4302. http://dx.doi.org/10.1529/biophysj.104.055855 PMID: 15778442

34. Gavutis M, Jaks E, Lamken P, Piehler J. Determination of the Two-Dimensional Interaction Rate Constants of a Cytokine Receptor Complex. Biophysical Journal. 2006; 90(9):3345–3355. http://dx.doi.org/10.1529/biophysj.105.072546 PMID: 16473899

35. Meyer M, Schneckener S, Ludewig B, Kuepfer L, Lippert J. Using expression data for quantification of active processes in physiologically based pharmacokinetic modeling. Drug Metabolism and Disposition. 2012; 40(5):892–901. https://doi.org/10.1124/dmd.111.043174 PMID: 22293118

36. Wills RJ, Dennis S, Spiegel HE, Gibson DM, Nadler PI. Interferon kinetics and adverse reactions after intravenous, intramuscular, and subcutaneous injection. Clinical Pharmacology & Therapeutics. 1984; 35:722–727. https://doi.org/10.1038/clpt.1984.101

37. Shah I, Band J, Samon HM, Young J, Robinson R, Bailey B, et al. Pharmacokinetics and tolerance of intravenous and intramuscular recombinant alpha 2 interferon in patients with malignancies. American journal of hematology. 1984; 17:363–71. https://doi.org/10.1002/ajh.2830170406 PMID: 6594039

38. Radwanski E, Perentesis G, Jacobs S, Oden E, Affrime M, Symchowicz S, et al. Pharmacokinetics of Interferon Î±-2b in Healthy Volunteers. The Journal of Clinical Pharmacology. 1987; 27(5):432–435. https://doi.org/10.1002/j.1552-4604.1987.tb03044.x PMID: 3693589

39. Cai Y, Zhang Z, Fan K, Zhang J, Shen W, Li M, et al. Pharmacokinetics, tissue distribution, excretion, and antiviral activity of pegylated recombinant human consensus interferon-variant in monkeys, rats and guinea pigs. Regulatory Peptides. 2012; 173(1):74–81. https://doi.org/10.1016/j.regpep.2011.09.008 PMID: 21985916

40. Bohoslawec O, Trown PW, Wills RJ. Pharmacokinetics and tissue distribution of recombinant human alpha A, D, A/D(Bgl), and I interferons and mouse alpha-interferon in mice. Journal of interferon research. 1986; 6(3):207–213. https://doi.org/10.1089/jir.1986.6.207 PMID: 3745986

41. Billiau A, Heremans H, Ververken D, van Damme J, Carton H, de Somer P. Tissue distribution of human interferons after exogenous administration in rabbits, monkeys, and mice. Archives of Virology. 1981; 68(1):19–25. https://doi.org/10.1007/BF01315163 PMID: 6166278

42. Johns TG, Kerry JA, Veitch BA, Mackay IR, Tutton PJ, Tymms MJ, et al. Pharmacokinetics, tissue distribution, and cell localization of [35S]methionine-labeled recombinant human and murine alpha interferons in mice. Cancer Research. 1990; 50(15):4718–4723. PMID: 2369745

43. Eigenmann MJ, Karlsen TV, Krippendorff BF, Tenstad O, Fronton L, Otteneder MB, et al. Interstitial IgG antibody pharmacokinetics assessed by combined in vivo- and physiologically-based pharmacokinetic modelling approaches. Journal of Physiology. 2017; 595(24):7311–7330. https://doi.org/10.1113/JP274819 PMID: 28960303

44. Maiwald T, Schneider A, Busch H, Sahle S, Gretz N, Weiss TS, et al. Combining theoretical analysis and experimental data generation reveals IRF9 as a crucial factor for accelerating *IFN–α*-induced early antiviral signalling; 2010. http://jjj.biochem.sun.ac.za/models/?id=maiwald.

45. Bolen CR, Ding S, Robek MD, Kleinstein SH. Dynamic expression profiling of type I and type III interferon-stimulated hepatocytes reveals a stable hierarchy of gene expression. Hepatology. 2014; 59(4):1262–1272. https://doi.org/10.1002/hep.26657 PMID: 23929627

46. Jilg N, Lin W, Hong J, Schaefer EA, Wolski D, Meixong J, et al. Kinetic differences in the induction of interferon stimulated genes by interferon-alpha and interleukin 28B are altered by infection with hepatitis C virus. Hepatology. 2014; 59(4):1250–1261. https://doi.org/10.1002/hep.26653 PMID: 23913866

47. Hucka M, Finney A, Sauro HM, Bolouri H, Doyle JC, Kitano H, et al. The systems biology markup language (SBML): a medium for representation and exchange of biochemical network models. Bioinformatics. 2003; 19(4):524–531. https://doi.org/10.1093/bioinformatics/btg015 PMID: 12611808

48. Kuepfer L, Peter M, Sauer U, Stelling J. Ensemble modeling for analysis of cell signaling dynamics. Nature Biotechnology. 2007; 25(9):1001–1006. https://doi.org/10.1038/nbt1330 PMID: 17846631

49. Schlaak JF, Hilkens CMU, Costa-Pereira AP, Strobl B, Aberger F, Frischauf AM, et al. Cell-type and donor-specific transcriptional responses to interferon-α: Use of customized gene arrays. Journal of Biological Chemistry. 2002; 277(51):49428–49437. https://doi.org/10.1074/jbc.M205571200 PMID: 12386168

50. Wolber EM, Haase B, Jelkmann W. Thrombopoietin production in human hepatic cell cultures (HepG2) is resistant to IFN-alpha, IFN-beta, and IFN-gamma treatment. Journal of interferon & cytokine research: the official journal of the International Society for Interferon and Cytokine Research. 2002; 22 (12):1185–1189. https://doi.org/10.1089/10799900260475704

51. Cordes H, Thiel C, Baier V, Blank LM, Kuepfer L. Integration of genome-scale metabolic networks into whole-body PBPK models shows phenotype-specific cases of drug-induced metabolic perturbation. npj Systems Biology and Applications. 2018; 4(1):10. https://doi.org/10.1038/s41540-018-0048-1 PMID: 29507756

52. Krauss M, Schaller S, Borchers S, Findeisen R, Lippert J, Kuepfer L. Integrating Cellular Metabolism into a Multiscale Whole-Body Model. PLoS Computational Biology. 2012; 8(10). https://doi.org/10.1371/journal.pcbi.1002750 PMID: 23133351

53. Theil C, Smit I, Baier V, Cordes H, Fabry B, Blank L, et al. Using quantitative systems pharmacology to evaluate the drug efficacy of COX-2 and 5-LOX inhibitors in therapeutic situations. npj SBA. 2018;.

54. Eissing T, Kuepfer L, Becker C, Block M, Coboeken K, Gaub T, et al. A computational systems biology software platform for multiscale modeling and simulation: Integrating whole-body physiology, disease biology, and molecular reaction networks. Frontiers in Physiology. 2011;FEB. https://doi.org/10.3389/fphys.2011.00004 PMID: 21483730

55. von Kleist Max, H W Kloft Charlotte, editor. Combining Systems Biology with physiologically-based pharmacokinetics to support the understanding of drug effects. vol. 231. Proceedings of Foundations of Systems Biology in Engeneering FOSBE; 2007.

56. Mager DE, Neuteboom B, Efthymiopoulos C, Munafo A, Jusko WJ. Receptor-mediated pharmacokinetics and pharmacodynamics of interferon-beta1a in monkeys. The Journal of pharmacology and experimental therapeutics. 2003; 306(1):262–70. https://doi.org/10.1124/jpet.103.049502 PMID: 12660309

57. Benson N, De Jongh J, Duckworth JD, Jones HM, Pertinez HE, Rawal JK, et al. Pharmacokinetic-pharmacodynamic modeling of alpha interferon response induced by a toll-like 7 receptor agonist in mice. Antimicrobial Agents and Chemotherapy. 2010; 54(3):1179–1185. https://doi.org/10.1128/AAC.00551-09 PMID: 20028817

58. Daud AI, Xu C, Hwu WJ, Urbas P, Andrews S, Papadopoulos NE, et al. Pharmacokinetic/pharmacodynamic analysis of adjuvant pegylated interferon α-2b in patients with resected high-risk melanoma. Cancer Chemotherapy and Pharmacology. 2011; 67(3):657–666. https://doi.org/10.1007/s00280-010-1326-9 PMID: 20509027

59. Kagan L, Abraham AK, Harrold JM, Mager DE. Interspecies scaling of receptor-mediated pharmacokinetics and pharmacodynamics of type I interferons. Pharmaceutical Research. 2010; 27(5):920–932. https://doi.org/10.1007/s11095-010-0098-6 PMID: 20232116

60. Nieforth KA, Nadeau R, Patel IH, Mould D. Use of an indirect pharmacodynamic stimulation model of MX protein induction to compare in vivo activity of interferon alfa-2a and a polyethylene glycol-modified derivative in healthy subjects. Clinical Pharmacology and Therapeutics. 1996; 59(6):636–646. https://doi.org/10.1016/S0009-9236(96)90003-X PMID: 8681488

61. Reddy KR. Development and pharmacokinetics and pharmacodynamics of pegylated interferon alfa-2a (40 kD); 2004.

62. Chatelut E, Rostaing L, Grégoire N, Payen JL, Pujol A, Izopet J, et al. A pharmacokinetic model for alpha interferon administered subcutaneously. British Journal of Clinical Pharmacology. 1999; 47 (4):365–371. https://doi.org/10.1046/j.1365-2125.1999.00912.x PMID: 10233199

63. Mager DE, Jusko WJ. Receptor-mediated pharmacokinetic/pharmacodynamic model of interferon-alpha 1a in humans. Pharmaceutical Research. 2002; 19(10):1537–1543. https://doi.org/10.1023/A:1020468902694 PMID: 12425473

64. Greenberg HB, Pollard RB, Lutwick LI, Gregory PB, Robinson WS, Merigan TC. Effect of human leukocyte interferon on hepatitis B virus infection in patients with chronic active hepatitis. The New England

journal of medicine. 1976; 295(10):517–22. https://doi.org/10.1056/NEJM197609022951001 PMID: 950957

65. Hawkins MJ, Borden EC, Merritt JA, Edwards BS, Ball LA, Grossbard E, et al. Comparison of the biologic effects of two recombinant human interferons alpha (rA and rD) in humans. Journal of Clinical Oncology. 1984; 2(3):221–226. https://doi.org/10.1200/JCO.1984.2.3.221 PMID: 6321691

66. Bornemann LD, Spiegel HE, Dziewanowska ZE, Krown SE, Colburn WA. Intravenous and intramuscular pharmacokinetics of recombinant leukocyte a interferon. European Journal of Clinical Pharmacology. 1985; 28(4):469–471. https://doi.org/10.1007/BF00544369 PMID: 4029251

67. Heim MH. In: Dufour JF, Clavien PA, editors. Interferon Signaling. Berlin, Heidelberg: Springer Berlin Heidelberg; 2010. p. 189–200. Available from: http://dx.doi.org/10.1007/978-3-642-00150-5_12.

68. Heim MH. 25 years of interferon-based treatment of chronic hepatitis C: an epoch coming to an end. Nat Rev Immunol. 2013; 13(7):535–542. https://doi.org/10.1038/nri3463 PMID: 23743475

69. Ivashkiv LB, Donlin LT. Regulation of type I interferon responses. Nature reviews Immunology. 2014; 14(1):36–49. https://doi.org/10.1038/nri3581 PMID: 24362405

70. Kuepfer L, Clayton O, Thiel C, Cordes H, Nudischer R, Blank LM, et al. A model-based assay design to reproduce in vivo patterns of acute drug-induced toxicity; 2018.

71. Thiel C, Cordes H, Conde I, Castell JV, Blank LM, Kuepfer L. Model-based contextualization of in vitro toxicity data quantitatively predicts in vivo drug response in patients. Archives of Toxicology. 2017; 91 (2):865–883. https://doi.org/10.1007/s00204-016-1723-x PMID: 27161439

72. Thiel C, Cordes H, Fabbri L, Aschmann HE, Baier V, Smit I, et al. A Comparative Analysis of Drug-Induced Hepatotoxicity in Clinically Relevant Situations. PLoS Computational Biology. 2017; 13(2). https://doi.org/10.1371/journal.pcbi.1005280 PMID: 28151932

73. Thiel C, Cordes H, Baier V, Blank LM, Kuepfer L. Multiscale modeling reveals inhibitory and stimulatory effects of caffeine on acetaminophen-induced toxicity in humans. CPT: Pharmacometrics and Systems Pharmacology. 2017; 6(2):136–146. https://doi.org/10.1002/psp4.12153 PMID: 28130915

74. Apweiler R, Beissbarth T, Berthold MR, Blüthgen N, Burmeister Y, Dammann O, et al. Whither systems medicine? Experimental & Molecular Medicine. 2018; 50(3):e453. https://doi.org/10.1038/emm.2017.290